Heliyon 8 (2022) e11187

Contents lists available at ScienceDirect

Heliyon

journal homepage: www.cell.com/heliyon

Research article

An improved U-net based retinal vessel image segmentation method

Kan Ren *, Longdan Chang, Minjie Wan, Guohua Gu, Qian Chen

Jiangsu Key Laboratory of Spectral Imaging and Intelligent Sense, Nanjing University of Science and Technology, Nanjing 210094, China

ARTICLE INFO

Keywords:
Retinal vessel segmentation
Deep learning
U-net
Bi-FPN

ABSTRACT

Diabetic retinopathy is not just the most common complication of diabetes but also the leading cause of adult blindness. Currently, doctors determine the cause of diabetic retinopathy primarily by diagnosing fundus images. Large-scale manual screening is difficult to achieve for retinal health screen. In this paper, we proposed an improved U-net network for segmenting retinal vessels. Firstly, due to the lack of retinal data, pre-processing of the raw data is required. The data processed by grayscale transformation, normalization, CLAHE, gamma transformation. Data augmentation can prevent overfitting in the training process. Secondly, the basic network structure model U-net is built, and the Bi-FPN network is fused based on U-net. Datasets from a public challenge are used to evaluate the performance of the proposed method, which is able to detect vessel SP of 0.8604, SE of 0.9767, ACC of 0.9651, and AUC of 0.9787.

1. Introduction

Accurate segmentation of the retinal vasculature is vital for diagnosing of many major diseases [1], for example, diabetes mellitus and hypertension. Often, in the early stages of the disease process, the retinal vessels develop lesions, such as Microaneurysms, excessive curvature, and narrowing of the vessels. In the early screening phase, the health of the retinal vessels can be determined by diagnosing their morphology. However, the large amount of imaging data increases the workload of physicians. The process is time-consuming and is accompanied by unavoidable manual errors (see Table 1).

Internationally, the use of artificial intelligence methods for assisted diagnosis is widespread. Artificial intelligence-aided diagnosis can avoid errors due to human operations and reduce the workload of imaging physicians, which helps the community identify diseases on a large scale. With the development of science and technology, deep learning has achieved remarkable results in various research fields. In the field of medical research, complex medical images can affect doctors' diagnoses. Moreover, deep learning is superior in image segmentation, image alignment, lesion detection, assisted diagnosis, and image histology biomarker extraction, which can overcome the difficulties of multiple differences in medical image types, complex fusion, low signal-to-noise ratio, and the variability of biological individuals.

Segmentation algorithms are classified into two categories according to the learning mode: supervised and unsupervised learning.

(1) Unsupervised learning refers to getting the relationship between data based on a specific model, such as clustering, anonymous data, and the relationship between features. Unsupervised learning can be generally divided into two categories: matched filtering methods and model-based methods. The matched filter-based segmentation algorithm uses the correlated information between the local image blocks and the filter kernel. It performs a two-dimensional convolution operation on the retinal image based on a two-dimensional Gaussian template to reproduce the vascular structure in both width and direction. Chaudhuri et al. [2] were the first to propose a two-dimensional matched filter approach for retinal vessel segmentation, approximating the retinal vessel cross-sectional map with a Gaussian curve. Azzopardi et al. [3] proposed to use several different convolution kernels to extract different filter features and then segment the blood vessels using the extracted features. Zhang et al. [4] proposed a multi-scale second-order Gaussian derivative filter in the maximized directional fractional domain based segmentation method. They evaluated the performance of their algorithm by using six publicly available datasets, and results was experimentally demonstrated that the method was able to segment the delicate vascular structures and cross-sections of vascular structures. The model-based approach includes a vessel profile model and a deformable model. In the vessel profile model, the profile of the vessel cross-sectional intensity is considered as a Gaussian curve. In the variability model, the primary profile method and

* Corresponding author.
E-mail address: k.ren@njust.edu.cn (K. Ren).

https://doi.org/10.1016/j.heliyon.2022.e11187
Received 9 March 2022; Received in revised form 4 August 2022; Accepted 17 October 2022

Table 1. Segmentation results of different algorithms.

Type	Methods	SE	SP	ACC	AUC
Unsupervised learning	Zana [13]	0.6971	—	0.9377	0.8984
	AI-Diri [14]]	0.7282	0.9551	—	—
	Miri [15]	0.7352	0.9795	0.9458	—
	Fraz [16]	0.7152	0.9795	0.9430	—
	You [17]	0.7410	0.9759	0.9434	—
Supervised learning	Fraz [18]	0.7152	0.9751	0.9430	—
	Marin [19]	0.7067	0.9769	0.9452	0.9588
	Ricci [20]	—	0.9801	0.9563	0.9558
	Sohini [21]	0.7249	—	0.9519	0.9620
	Oliveira [22]	0.8039	0.9804	0.9576	0.9821
	Alom [23]	0.7792	0.9813	0.9556	0.9784
	U-NET	0.7240	0.9848	0.9516	0.9735
	Tamim [27]	0.7542	0.9843	0.9607	—
	This article	0.8064	0.9767	0.9551	0.9787

the level set-based method were used. It is generally considered that the cross-sectional shape of the blood vessel conforms to a Gaussian distribution. Since the model gives poor segmentation results for low-resolution images, Gang et al. proposed an improved approach based on the above model, using Gaussian difference for modeling. Gonzalez et al. [5] proposed a joint framework for not only retinal vessel but also optic disc segmentation, which uses a graph cut method for segmenting the vessel tree, followed by a Markov random field graph construction, and a compensation factor method disc segmentation was performed.

(2) Supervised learning refers to training to obtain an optimal model based on a known relationship between the input and output of a data set, with both features and labels on the training data. Supervised learning algorithms classify each pixel and determine whether the pixel belongs to the vessel or the background. In general, supervised methods tend to perform better than unsupervised methods. In [6], support vector machine (SVM) classifiers were proposed to be trained using manually designed features, which showed a significant performance improvement compared to unsupervised algorithm segmentation results. However, such methods are based on hand-designed features and have poor generalization ability. In the research field of machine or deep learning, many excellent algorithms have shown excellent performance on publicly available datasets. In 2016, Laskowski et al. [7] proposed a geometric transform-based data augmentation for training CNN networks to achieve vascular segmentation. Lahiri et al. [8] proposed an auto-encoder-based inheritance network architecture that implements vascular segmentation by combining all auto-encoder outputs. To achieve vascular segmentation. Maji et al. [9] utilized an ensemble of 12 deep CNN networks and averaged the outputs of all networks as the final input. Deep retinal images understood VGGNet [10] as the basis for effectively solving retinal vascular and optic disc segmentation using a whole convolutional network with two specific layers.

Compared with traditional algorithms, deep learning reduces human intervention, builds better prediction models, and avoid bias due to the lack of data.

This paper proposes an improved U-net model for retinal vessel segmentation to address the shortcomings of the algorithms mentioned above. Firstly, the data are pre-processed, and CLAHE performs image enhancement, and then the enhanced image is sliced. The processed data are fed into the network based on the U-net model and fused with the Bi-FPN fusion network in the Efficient Det network. The fused network fuses the features at the bottom layer with the features at the top layer, thus improving the accuracy of accurate vessel segmentation. The results of our experiments demonstrate that the network achieves better performance on the retinal vessel segmentation task.

2. Methods

In this section, our proposed segmentation method will be described in detail. The preprocessing includes grayscale transformation, normalization, CLAHE, and gamma transformation in the training phase. To increase the number of training samples, we use a slicing method to slice the original image into small-sized image blocks of uniform size and augmented samples as the input to the network.

2.1. Pre-processing

Fundus images have disadvantages such as uneven brightness, poor contrast, and strong noise, requiring per-processing before input the network for training. Figures 1(A) and 1(B) show the original fundus image and manually labeled vascular map of the retinal vessels.

The fundus images are converted to grayscale and then normalized. The conversion equation is shown as follows:

$$I_{gray} = 0.299 \times I_r + 0.587 \times I_g + 0.114 \times I_b \tag{1}$$

Among them I_r, I_g andI_b are the RGB channel components of fundus images. As shown in Eq. (1), I_{gray} is the result of processing. It is standardized and the standardization equation is shown in Eq. (2).

$$I_{norm} = \frac{I_{gray} - \mu}{\sigma} \tag{2}$$

Among them, μ denotes the mean value,σ denotes variance.

Figure 2(B) is the gray scale of Figure 2(A).

Data augmentation can increase amount of the samples in the training set, effectively alleviating model overfitting, and bringing stronger generalization ability to the model. Data augmentation is generally divided into three categories: geometric transformations, color space transformations, and pixel point operations. Cropping is a common method among geometric transformations and a long, more obvious way to enhance data, which can augment data without destroying the accuracy condition. In this paper, based on this cropping property, we choose to augment the data by random slicing.

The retinal dataset used in this paper contains 20 training sets and 20 test sets. To fit our improved network structure, the original images need to be chunked. The patches which have been segmented are merged to create the segmented blood vessel image at the end of the procedure.

The original image 565*565 is sliced into 48*48 size patches, as shown in Figure 3, each obtained by randomly selecting its center within the image. Some patches are located in the circular field of view, some patches are located outside the circular field of view, and others are located above the boundary. In this way, not only the dataset is enlarged, but also the network can learn how to distinguish FOV boundaries.

2.2. Image enhancement

As shown in Figure 4(A)&(B), we use CLAHE (Contrast Limited Adaptive Histogram Equalization) for image enhancement. The adaptive histogram equalization algorithm expands the local contrast and displays smooth details by performing histogram equalization in a rectangular area around the currently processed pixel. Fortunately, CLAHE can effectively limit the noise amplification generated in the process of contrast expansion. It mainly contains image chunking, block linear interpolation, and layer filtering, and blending operations with the original image.

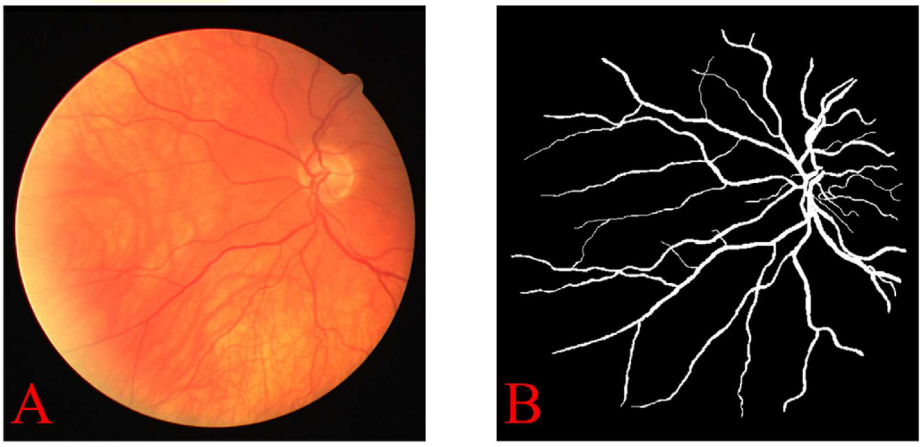

Figure 1. Original fundus image (A) and Manually labeled vascular map of the retinal vessels (B).

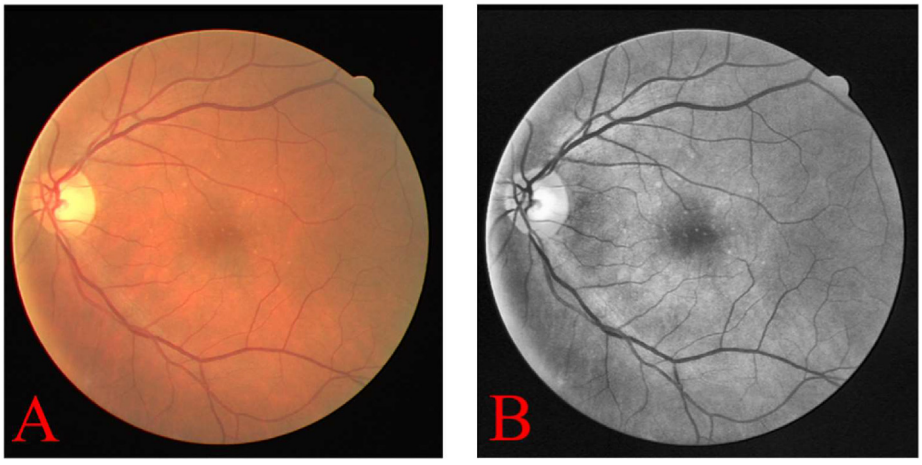

Figure 2. Original (A) and Grayscale (B) fundus image.

2.3. U-net

The U-net consists of an input layer, a hidden layer, and an output layer. Its structure is shown in Figure 5. The hidden layer can be divided into an up-sampling and a down-sampling part, distinguishing decoders and encoders. Down-sampling consists of convolution layer and pooling layer, which play the role of path shrinking in the network and capture global information. The up-sampling consists of convolutional and deconvolution layers, which play the role of path expansion in the network and locate pixel points. The output layer is an end-to-end network that classifies each pixel point of the feature map with the same size as the original image after up-sampling by the softmax [12] activation function. That is, the input image is of the same size as the output image.

2.4. Bi-FPN

The down-sampling layer part of the U-net network is used to extract the features of the image. After several operations such as convolution and maximum pooling, it makes the shallow layer information lost, which is the main reason for the degradation of segmentation accuracy. In order to combine the high and low resolution information better, this paper incorporates the Bi-FPN network into the U-net network to form a new network structure.

The main task of multi-scale feature fusion is to combine features at different scales of resolutions and can improve segmentation performance efficiently. Low-level features have better resolution and contain more information on location and detail. High-level features have low resolution and poor perception of details. The way to efficiently fuse the features from different levels is the key to optimize the segmentation model.

Model efficiency is crucial in computer vision. Bi-FPN is proposed to pursue a more efficient multi-scale fusion method. Bi-FPN is used to replace the skip connection, and the concept of weight is proposed to balance the feature information of various scales better and improve the efficiency of the model. The higher level of semantic information is more able to help us segment the target accurately. Some of the fine target information may be ignored when doing down-sampling operation in deep images. The proposed multi-scale feature fusion network is a good solution to this problem.

$O = \sum_i \frac{\omega_i}{\varepsilon + \sum_j \omega_j} \cdot I_i$, we are implementing a ReLU procedure after every ω_i, by using $\omega_i \geq 0$ and in order to maintain stability of numerical values, we set $\varepsilon = 0.0001$ at a small value. Additionally, normalized exponential function is not implemented in this procedure, and the weight value of each normalized parameters is between range 0–1, so the efficiency of this procedure is still very impressive [26].

The bidirectional cross-scale connections and the fast-normalized fusion are both included in the Bi-FPN. In order to simplify the example, at level 6, we demonstrated the two fused features for Bi-FPN. As shown in Figure 6, the structure diagram shows the computational steps in the middle of connecting each shallow feature to the output feature of the corresponding height [26].

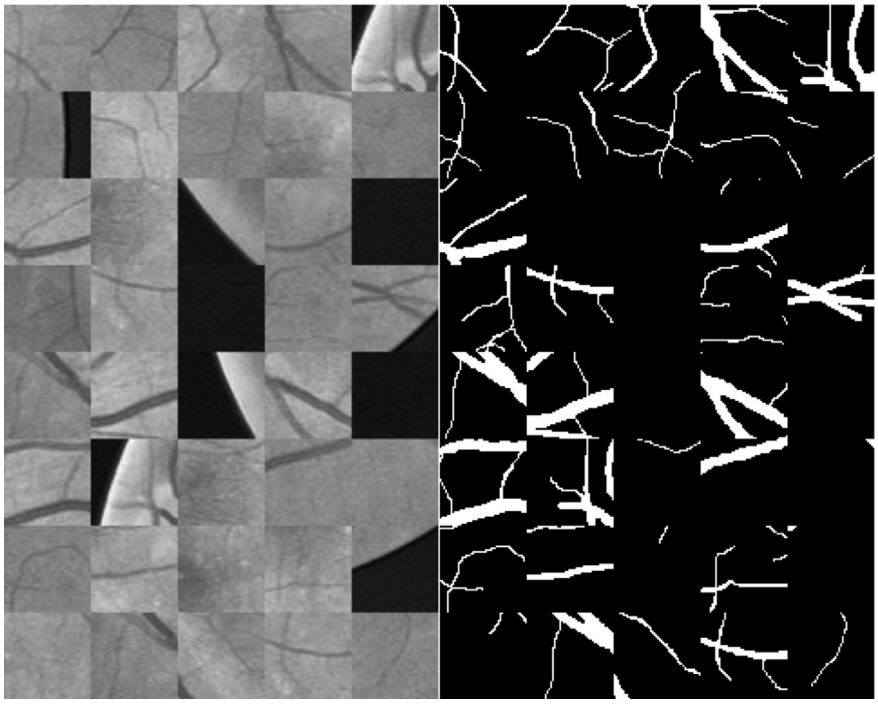

Figure 3. Data amplification.

$$P_6\_td = Conv\left(\frac{\omega_1 \cdot P_6\_in + \omega_2 \cdot Resize(P_7\_in)}{\omega_1 + \omega_2 + \varepsilon}\right) \tag{3}$$

$$P_6\_out = Conv\left(\frac{\omega_1' \cdot P_6\_in + \omega_2' \cdot P_6\_td + \omega_3' \cdot Resize(P_5\_out)}{\omega_1' + \omega_2' + \omega_3' + \varepsilon}\right) \tag{4}$$

As shown in Eqs. (3) and (4), the intermediate characteristic parameters P_6_td is at level 6 on the top to bottom route, and characteristic parameters P_6_out of the output is at same level as P_6_td but on the bottom to top path. The other features are performed in a similar manner. We use depth wise separable convolution [24, 25] first for feature fusion, then implement batch normalization and activation after each convolution [18, 26] to boost the efficiency.

Batch Normalization**.** With the increasing amount of neural network layers, the networks need to learned more parameters. During the training of U-net network, the data distribution of the subsequent network layer will change with the parameters of the previous layer [29]. With the deepening of the network layer, these adverse changes are amplified and may reduce the speed of network convergence. In order to defeat this shortcoming, BN layer was implemented before using ReLU procedure [28]. BN layer can standardize and evenly distribute the network layer data, and these new data will not have a significant impact on subsequent layers, which can improve the convergence efficiency of the network. In addition, BN layer has the effect of regularization, which takes a positive effective for the transmission of gradient feedback, and can help network avoid the over-fitting [29].

The neural network structure built in this paper is based on U-net structure and Bi-FPN, which can extract blood vessels more effectively. The network structure is shown in Figure 7. It uses U-net as the backbone network and Bi-FPN as the feature network to transfer shallow information at the input end down to the output end of the corresponding height. The improved network structure inherits the symmetric structure of the U-net network, and the hidden layer is also composed of up-sampling and down-sampling parts. The difference is that the Bi-FPN network can better fuse contextual detail features in the overall structure to avoid poor segmentation accuracy.

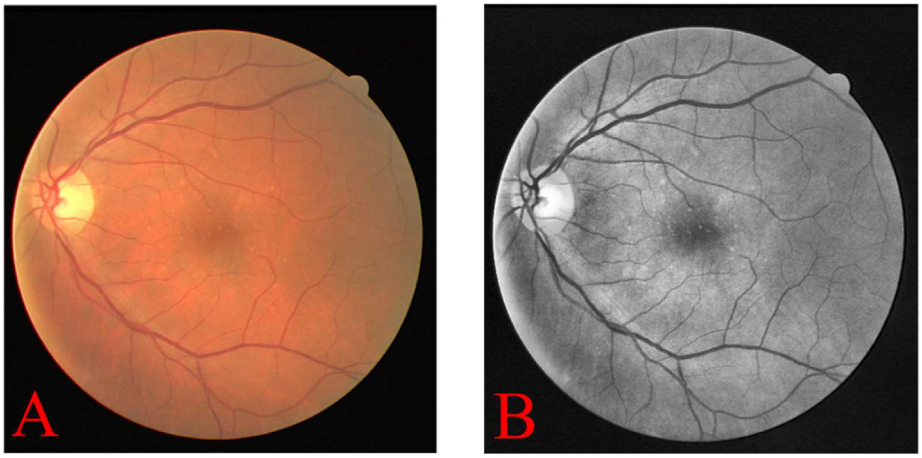

Figure 4. Original (A) and Enhanced (B) fundus image.

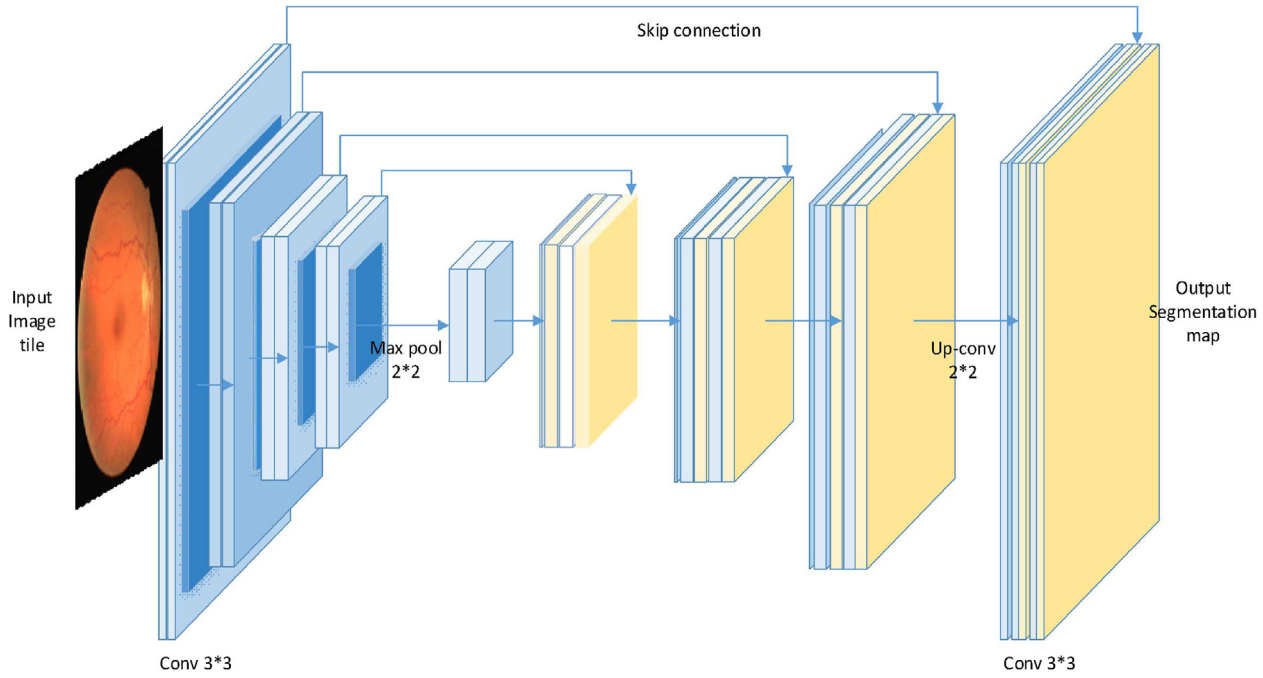

Figure 5. U-net structure.

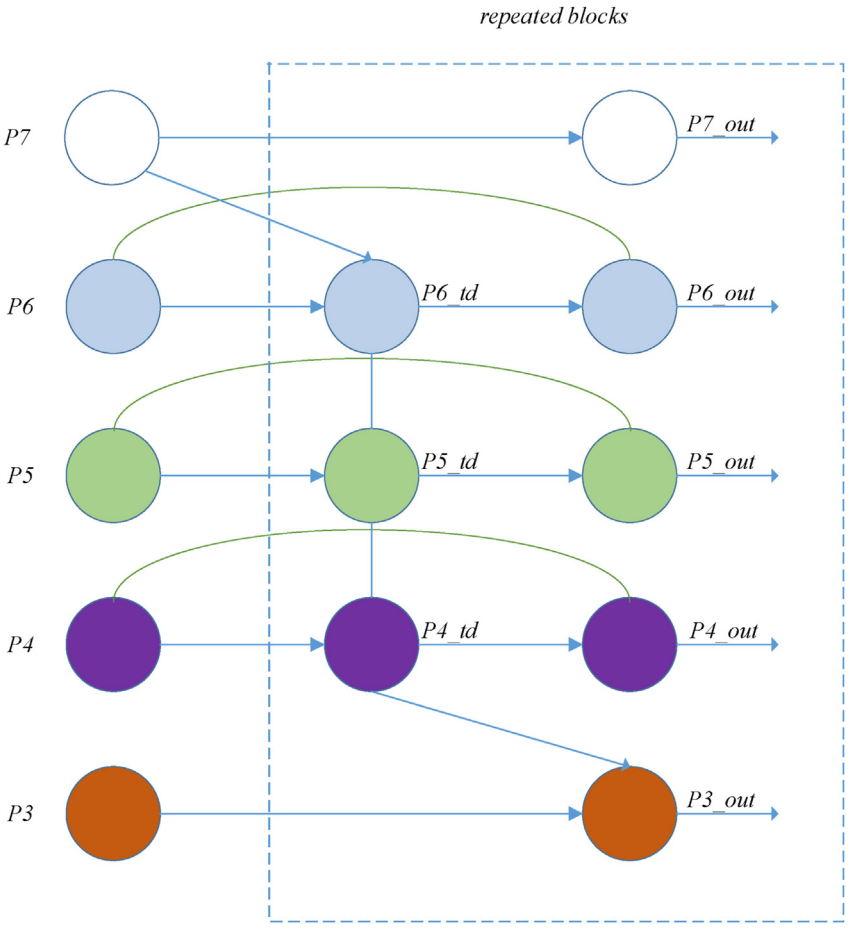

Figure 6. Bi-FPN structure.

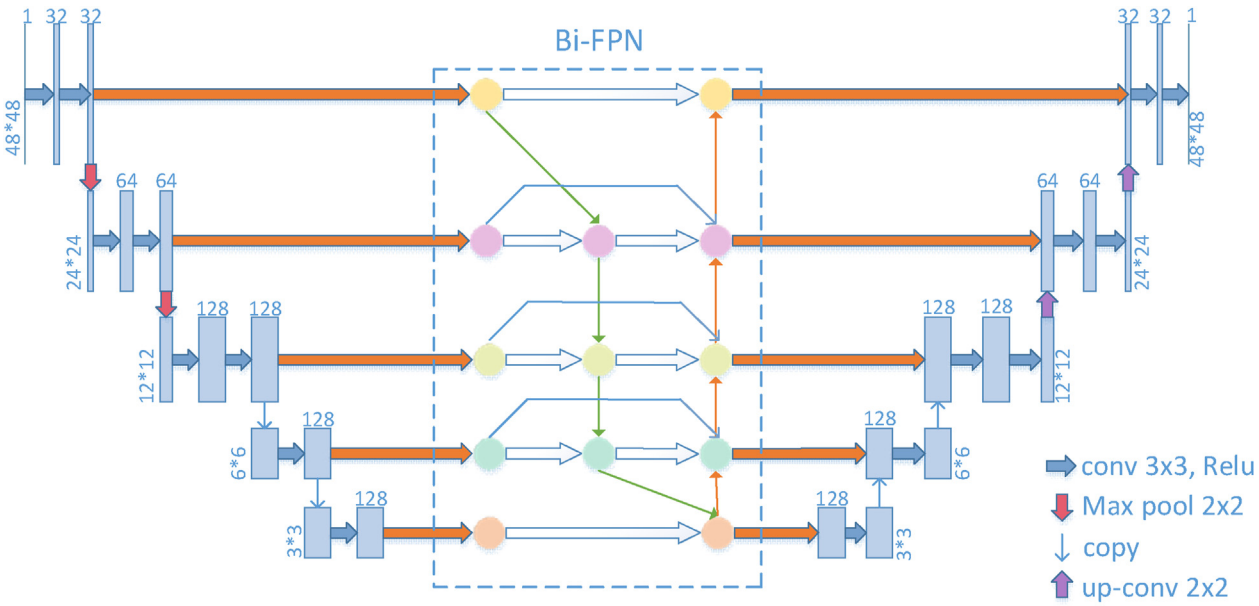

Figure 7. Unet-Bi-FPN network model.

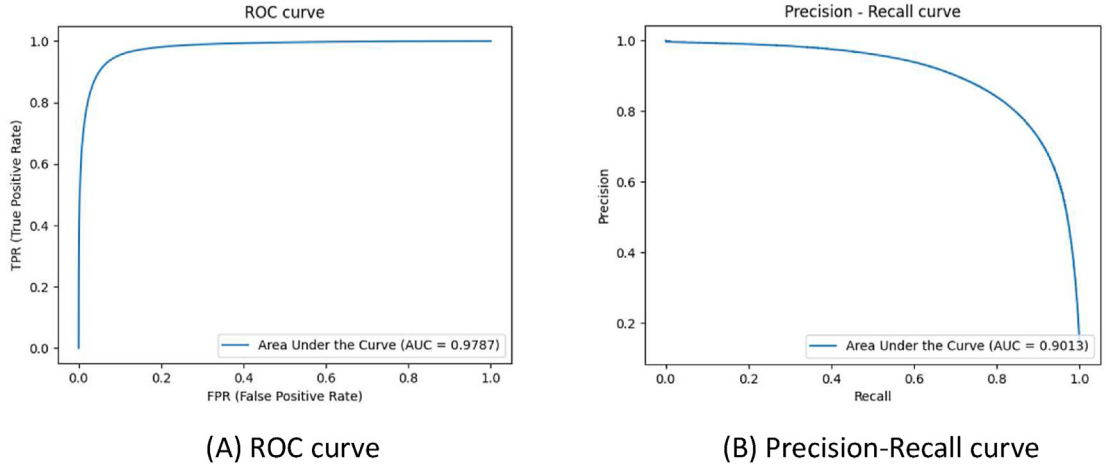

Figure 8. Evaluation index: ROC curve (A) and Precision-Recall curve (B).

3. Experiments

3.1. Datasets

In this paper, we use the DRIVE [11] dataset. Images in the DRIVE dataset were obtained from the Dutch Diabetic Retinal Screening Program, using fundus images obtained with a 45-degree field of view (FOV) Canon CR5 non-dilated 3CCD camera. The size of each fundus image is 768 × 584 8-bit color images. The FOV of each image in the dataset is circular with a diameter of 540 pixels, and the corresponding FOV image is given as a masked image. Among them, 33 are standard retinal images, 7 have mild lesions, and each image has a gold standard segmented by hand by experts.

3.2. Experimental process

In model training, 20 images of the training set are sliced and divided into 19000 patches, and 90% of them are selected for training in each training round, and the remaining 10% are used for validation. After slicing, the size of the images is 48*48 pixels, and the information of its color space is retained, and the size is 48*48*3.

In this paper, the categorical cross-entropy function is used as the loss function. As shown in Eq. (5), the cross-entropy evaluates how the probability distribution obtained from the current training differs from the actual distribution.

$$loss = -\sum_{i=1}^{n} \widehat{y_{i1}} \log y_{i1} + \widehat{y_{i2}} \log y_{i2} + \ldots + \widehat{y_{im}} \log y_{im} \tag{5}$$

3.3. Evaluation methodology

Experiments were conducted to analyze and compare the performance of the segmentation algorithm proposed in this paper with other algorithms using evaluation indexes such as accuracy, sensitivity, specificity, precision, and AUC, which are defined as follows:

$$ACC = \frac{TP + TN}{TP + TN + FP + FN} \tag{6}$$

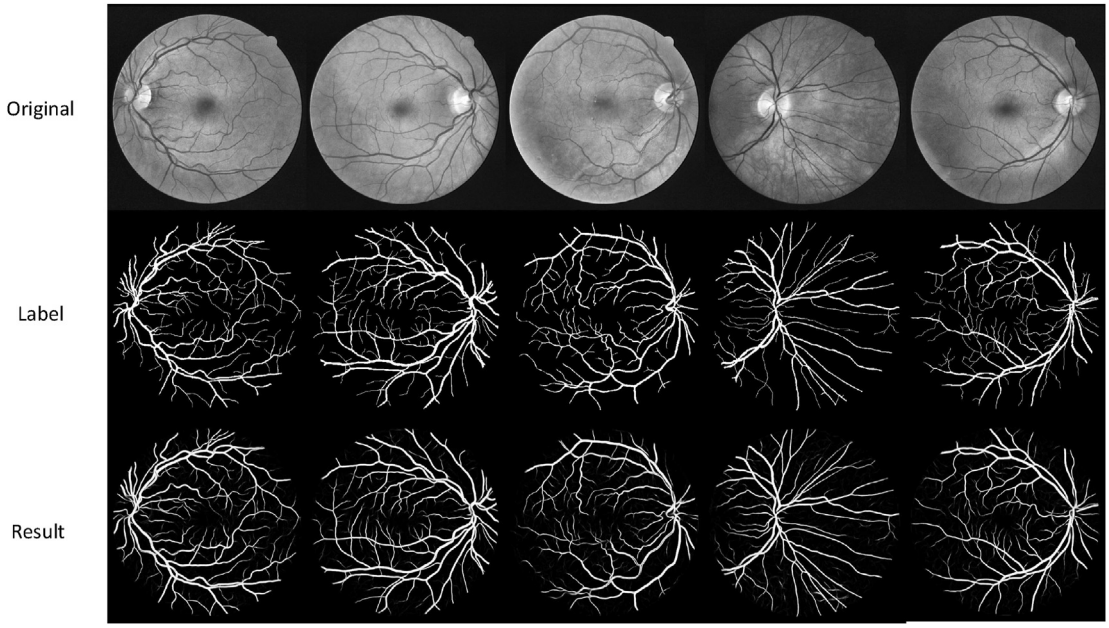

Figure 9. Comparison chart of experimental results.

$$Precision = \frac{TP}{TP + FP} \tag{7}$$

$$Recall = \frac{TP}{TP + FP} \tag{8}$$

TP (True Positive), FP (False Positive), FN (False Negative), TN (True Negative).

As shown in Eqs. (6), (7), and (8), we can see the relationship between evaluation index and TP、FP、FN、TN.

As we can find in Figure 8 (A) ROC curve: It is a composite index reflecting the continuous variables of sensitivity and specificity, and each point on the curve reflects the perceptibility to the same signal stimulus. And as we can find in Figure 8 (B) Precision-Recall curve: Take the precision rate as the y-axis and the recall rate as the x-axis. The higher the precision rate and the higher the recall rate, the more efficient the model algorithm is proved to be, i.e., the closer the curve is to the upper right corner.

In this paper, the model training cycles are 20, and each cycle takes about 41 s. The original U-net model has 150 training cycles, about 135 s per training cycle. This experiment runs on a computer platform with Windows 10 and Anaconda as the operating system, 3.6GHz Intel(R) HD Graphics 630 as the processor, NVIDIA TITAN Xp as the graphics card, and 32GB of memory from Kingston. the experiment runs on Python 3.8 as the programming language and Tensorflow 2.3.1 as the deep learning framework. Tensorflow 2.3.1. The model in this paper has reduced training time, mainly because the Bi-FPN network can fuse the contextual feature details, which enables the model to segment the results closer to the labels in the initial training so that a higher accuracy can be achieved in the next training.

As can be seen from Figure 9, the performance of the algorithm in this paper can basically segment all the retinal vessels compared to the labeled map, and there are no missed and false detections at the turns and ends of the vessels.

4. Conclusion

Semantic segmentation is an important branch of image processing and machine vision. It classifies and judges each pixel of an image to achieve accurate segmentation. U-net is a simple and efficient segmentation model, which is suitable for training small data sets. In this paper, we use the U-net network as the backbone network and replace the skip connection with Bi-FPN to obtain a new neural network structure. Experiments proved that the algorithm proposed in this paper is outstanding in terms of sensitivity and accuracy when compared with other algorithms under the public dataset DRIVE. We are confident that the improved U-net architecture proposed in this paper can be more suitable for medical image segmentation.

Declarations

Author contribution statement

Kan Ren, Longdan Chang: Conceived and designed the experiments; Performed the experiments; Analyzed and interpreted the data; Contributed reagents, materials, analysis tools or data; Wrote the paper.

Minjie Wan, Guohua Gu, Qian Chen: Conceived and designed the experiments; Performed the experiments; Analyzed and interpreted the data; Contributed reagents, materials, analysis tools or data.

Funding statement

Dr. Kan Ren was supported by National Natural Science Foundation of China [62175111], Fundamental Research Funds for the Central Universities [30922010715].

Data availability statement

Data included in article/supp. material/referenced in article.

Declaration of interest's statement

The authors declare no conflict of interest.

Additional information

No additional information is available for this paper.

References

[1] T.Y. Wong, R. Klein, A.R. Sharrett, et al., Retinal arteriolar diameter and risk for hypertension[J], Ann. Intern. Med. 140 (4) (2004) 248–255.

[2] S. Chaudhuri, S. Chatterjee, N. Katz, et al., Detection of blood vessels in retinal images using two-dimensional matcher filters[J], IEEE Trans. Med. Imag. 8 (3) (1989) 263–269.
[3] G. Azzopardi, N. Strisciuglio, M. Vento, et al., Traniable COSFIRE filters for vessel delineation with application in retinal images[J], Med. Image Anal. 19 (1) (2015) 46–57.
[4] J. Zhang, B. Dashtbozorg, E. Bekkers, Robust Retinal Vessel Segmentation via Locally Adaptive Derivative Frames in Orientation Scores[J], IEEE Transactions on Medical Imaging 35 (12) (2016) 2631–2644.
[5] A. Salazar-Gonzalez, D. Kaba, Y. Li, Segmentation of blood vessels and optic disc in retinal images[J], IEEE Journal of Bio-medical and Health Informatics 18 (6) (2014) 1874–1886.
[6] M.M. Fraz, S.A. Barman, P. Remagnino, et al., An approach to localize the retinal blood vessels using bit planes and centerline detection[J], Comput. Methods Progr. Biomed. 108 (2) (2012) 600–616.
[7] D. Marin, M.E. Gegundez-Arias, B. Ponte, et al., An exudate detection method for diagnosis risk of diabetic macular edema in retinal images using feature-based and supervised classification[J], Med. Biol. Eng. Comput. 56 (8) (2018) 1379–1390.
[8] E. Ricci, R. Perfetti, Retinal blood vessel segmentation using line operators and support vector classification[J], IEEE Trans. Med. Imag. 26 (10) (2007) 1357–1365.
[9] R. Sohini, D.D. Koozekanani, K.K. Parhi, Blood vessel segmentation of fundus images by major vessel extraction and subimage classification[J], IEEE Journal of Biomedical and Health Informatics 19 (3) (2015) 1118–1128.
[10] A. Oliveira, S. Pereira, C.A. Silva, Retinal vessel segmentation based on fully convolutional neural networks [J], Expert Syst. Appl. 112 (2018) 229–242.
[11] J. Staal, M.D. Abramoff, NIEMEIJER, et al., Ridge-based vessel segmentation in color images of the retinal[J], IEEE Trans. Med. Imag. 23 (4) (2004) 501–509.
[12] A.A. Nahid, M.A. Mehrabi, Y.N. Kong, Histopathoiogical Breast Cancer Image Classification by Deep Neural Network Techniques Guided by Local clustering[J], 2018, BidMed Research International, 2018, p. #2362108.
[13] F. Zana, J.C. Klein, Segmentation of vessel-like petterns using mathematical morphology and curvature evaluation[J], IEEE Trans. Image Process. 10 (7) (2001) 1010–1019.
[14] B. Al-Diri, A. Hunter, D. Steel, An active contour model for segmenting and measuring retinal vessels[J], IEEE Trans. Med. Imag. 28 (9) (2009) 1488–1497.
[15] M.S. Miri, A. Mahloojifar, Retinal image analysis using curvelet transform and multistructure elements morphology by reconstruction[J], IEEE (Inst. Electr. Electron. Eng.) Trans. Biomed. Eng. 58 (5) (2011) 1183–1192.
[16] M.M. Fraz, S.A. Barman, P. Remagnino, et al., An approach to localize the retinal blood vessels using bit planes and centerline detection[J], Comput. Methods Progr. Biomed. 108 (2) (2012) 600–616.
[17] X.G. You, Q.M. Peng, Y. Yuan, et al., Segmentation of retinal blood vessels using the radial projection and semi-supervised approach[J], Pattern Recogn. 44 (10-11) (2011) 2314–2324.
[18] M.M. Fraz, P. Remagnino, A. Hoppe, et al., Blood vessel segmentation methodologies in retinal images: a survey[J], Comput. Methods Progr. Biomed. 108 (1) (2012) 407–433.
[19] D. Marin, M.E. Gegundez-Arias, B. Ponte, et al., An exudate detection method for diagnosis risk of diabetic macular edema in retinal images using feature-based and supervised classification[J], Med. Biol. Eng. Comput. 56 (8) (2018) 1379–1390.
[20] E. Ricci, R. Perfetti, Retinal blood vessel segmentation using line operators and support vector classification[J], IEEE Trans. Med. Imag. 26 (10) (2007) 1357–1365.
[21] R. Sohini, D.D. Koozekanani, K.K. Parhi, Blood vessel segmentation of fundus images by major vessel extraction and subimage classification[J], IEEE Journal of Biomedical and Health Informatics 19 (3) (2015) 1118–1128.
[22] A. Oliveira, S. Pereira, C.A. Silva, Retinal vessel segmentation based on fully convolutional neural networks[J], Expert Syst. Appl. 112 (2018) 229–242.
[23] Alom M Z, Hasan M, Yakopcic C, et al. Recurrent Residual Convolutional Neural Network Based on U-Net (R2U-Net) for medical image segmentation [DB/OL].
[24] Francois Chollet, Xception: Deep Learning with Depthwise Separable Convolutions. CVPR, 2017, pp. 1610–2357.
[25] Sifre Laurent, Rigid-motion scattering for image classification, Ph.D. thesis section 6 (2) (2014).
[26] M. Tan, R. Pang, Q.V. Le, EfficientDet: scalable and efficient object detection, IEEE/CVF Conference on Computer Vision and Pattern Recognition (CVPR) (2020) 10778–10787.
[27] N. Tamim, G. Azim, H. Nassar, Retinal blood vessel segmentation using hybrid features and multi-layer perceptron neural networks, Symmetry 12 (2020) 894.
[28] S. Ioffe, C. Szegedy, Batch normalization:accelerating deep network training by reducing internal covarite shift, Lille, France, ICML 2015 Proceedings of the 32nd International Conference on Machine Learning – Volume 37 (2015) 448–456.
[29] Y. Cai, Y. Li, X. Gao, Y. Guo, Retinal vessel segmentation method based on improved deep U-net, in: Z. Sun, R. He, J. Feng, S. Shan, Z. Guo (Eds.), Biometric Recognition. CCBR 2019. Lecture Notes in Computer Science 11818 (2019) 321–328. Springer, Cham.